NeuroImage: Clinical 14 (2017) 216–221

Contents lists available at ScienceDirect

NeuroImage: Clinical

journal homepage: www.elsevier.com/locate/ynicl

# Simultaneous investigation of microvasculature and parenchyma in cerebral small vessel disease using intravoxel incoherent motion imaging

Sau May Wong[a,c,1], C. Eleana Zhang[b,c,d,1], Frank C.G. van Bussel[a,c], Julie Staals[b,d], Cécile R.L.P.N. Jeukens[a], Paul A.M. Hofman[a,c], Robert J. van Oostenbrugge[b,c,d], Walter H. Backes[a,c], Jacobus F.A. Jansen[a,c,*]

[a] Dept. of Radiology & Nuclear Medicine, Maastricht University Medical Centre, Maastricht, The Netherlands
[b] Dept. of Neurology, Maastricht University Medical Centre, Maastricht, The Netherlands
[c] School for Mental Health and Neuroscience (MHeNs), Maastricht University Medical Centre, Maastricht, The Netherlands
[d] Dept. of Cardiovascular Research Institute Maastricht (CARIM), Maastricht University Medical Centre, Maastricht, The Netherlands

ARTICLE INFO

*Article history:*
Received 18 August 2016
Received in revised form 28 November 2016
Accepted 16 January 2017
Available online 17 January 2017

*Keywords:*
Cerebral small vessel disease
Intravoxel incoherent motion imaging
Diffusion weighted imaging
Perfusion MR imaging
Microvasculature
Brain parenchyma

ABSTRACT

*Introduction:* Cerebral small vessel disease (cSVD) is associated with microvascular and parenchymal alterations. Intravoxel incoherent motion (IVIM) MRI has been proposed to simultaneously measure both the microvascular perfusion and parenchymal diffusivity. This study aimed to evaluate the application of IVIM in cSVD to assess the microvasculature and parenchymal microstructure.

*Methods:* Seventy-three patients with cSVD (age 70 ± 11 y) and thirty-nine controls (age 69 ± 12 y) underwent IVIM imaging (3T). Group differences of the perfusion volume fraction $f$ and the parenchymal diffusivity $D$ were investigated using multivariable linear regression accounted for age, sex and cardiovascular factors. To examine the relation between the IVIM measures and the disease severity on structural MRI, white matter hyperintensity (WMH) load served as surrogate measure of the disease severity.

*Results:* Patients had a larger $f$ ($p < 0.024$) in the normal appearing white matter (NAWM) than controls. Higher $D$ ($p < 0.031$) was also observed for patients compared with controls in the NAWM and grey matter. Both $f$ ($p < 0.024$) and $D$ ($p < 0.001$) in the NAWM and grey matter increased with WMH load.

*Conclusions:* The increased diffusivity reflects the predicted microstructural tissue impairment in cSVD. Unexpectedly, an increased perfusion volume fraction was observed in patients. Future studies are needed to reveal the precise nature of the increased perfusion volume fraction. IVIM imaging showed that the increases of $f$ and $D$ in cSVD were both related to disease severity, which suggests the potential of IVIM imaging to provide a surrogate marker for the progression of cSVD.



## 1. Introduction

Age and vascular risk factor related cerebral small vessel disease (cSVD) is a common microvascular pathology underlying burdensome diseases like lacunar stroke and vascular cognitive impairment (Pantoni, 2010; Makin et al., 2013; Pantoni & Gorelick, 2011). Alterations in the parenchyma have been described in cSVD as structural MRI abnormalities like lacunes, white matter hyperintensities, microbleeds and enlarged perivascular spaces (PVS) (Wardlaw & Smith, 2013). However, little is known about the precursors of these alterations, although MRI has provided some insight in this. Using perfusion MRI, hypoperfusion was found for the white matter in patients with cSVD (Markus et al., 2000; O'Sullivan et al., 2002). Diffusion weighted imaging studies have provided indications that the loss of microstructural integrity in the white matter may be associated with cSVD (Jones et al., 1999; Chabriat et al., 1999; O'Sullivan et al., 2001). Parallel data of the microvasculature and the parenchyma in the same patient group are lacking. More pathophysiological insights may be obtained by evaluating both structures concurrently and by linking them together.

Intravoxel incoherent motion (IVIM) imaging is a non-invasive MRI technique that proposes to simultaneously measure such microvascular and parenchymal microstructural tissue properties (Le Bihan et al., 1988). In contrast to conventional diffusion weighted techniques, where the microvascular signal confounds the parenchymal signal, it is assumed that IVIM can separate the MRI effects of the

*Abbreviations:* BMI, body mass index; cSVD, cerebral small vessel disease; DGM, deep grey matter; DW, diffusion weighted; FOV, field of view; FLAIR, fluid attenuated inversion recovery; IVIM, intravoxel incoherent motion imaging; LS, lacunar stroke; mVCI, mild vascular cognitive impairment; NAWM, normal appearing white matter; PVS, perivascular spaces; ROI, region of interest; SNR, signal-to-noise ratio; WMH, white matter hyperintensity.

* Corresponding author at: Department of Radiology & Nuclear Medicine, Maastricht University Medical Centre, PO Box 5800, 6202 AZ Maastricht, The Netherlands.
*E-mail address:* jacobus.jansen@mumc.nl (J.F.A. Jansen).

[1] Both authors contributed equally to this work.

http://dx.doi.org/10.1016/j.nicl.2017.01.017

microvasculature and parenchyma. Promising results of IVIM in various clinical applications (e.g. oncology (tumor staging) and neuroimaging (management of cerebral infarction)) have been shown (Iima & Le Bihan, 2016). The purpose of the present study was to investigate the applicability of IVIM in cSVD by assessing the microvasculature and parenchymal microstructure.

## 2. Methods

### 2.1. Standard protocol approvals, registrations and patient consents

This is a retrospective study and has been approved by the Medical Ethics Committee of Maastricht University Medical Centre. All participants were included after written informed consent was obtained.

### 2.2. Study population

Between April 2013 and December 2014, 83 patients with clinically manifest cSVD and 40 healthy controls were included. Participants were included from the Maastricht University Medical Centre and Zuyderland Medical Centre, The Netherlands. Clinically manifest cSVD was defined as the occurrence of a recent lacunar stroke or the diagnosis of mild vascular cognitive impairment (mVCI) due to cSVD.

Patients with lacunar stroke (n = 44) had a first-ever acute lacunar syndrome with a compatible recent small subcortical infarct on brain MRI (Wardlaw et al., 2013a). If no such lesion was visible on imaging, established clinical criteria for lacunar syndrome were used (Appendix 1.1) (Bamford et al., 1987). Exclusion criteria for these patients include a potential cardiac embolic source (e.g. atrial fibrillation), or stenosis of ≥50% of one or both internal carotid arteries. Patients were included 3 months after the acute stroke to avoid acute stroke phase changes.

Patients with mVCI (n = 39) had subjective cognitive complaints, failure in one or more cognitive domains determined by neuropsychological assessment, and extensive MRI abnormalities associated with cSVD, i.e. white matter hyperintensities (WMHs) Fazekas score 3 or Fazekas score 2 or 3, and/or with microbleeds, and/or lacunes and no other apparent cause for the cognitive deficits (Gorelick et al., 2011). Furthermore, participants in whom a neurodegenerative disease other than vascular cognitive impairment was suspected (e.g. Alzheimer's disease), with another neurological or psychiatric disease interfering with cognitive testing or with severe cognitive impairment defined as Mini Mental State Examination <20 and/or Clinical Dementia Rating >1, were excluded.

Controls (n = 40) were stroke-free and had back pain or peripheral neuropathies without (subjective) cognitive failures. Controls were matched on age and sex.

All participants with a history of cerebrovascular disease, or other diseases of the central nervous system or with MRI contraindications were excluded. Baseline characteristics were recorded, including age, sex, education (Verhage, 1964), and cardiovascular factors such as hypertension (history of hypertension/antihypertensive medicine (including calcium antagonists)), hypercholesterolemia (history of hypercholesterolemia/statin), diabetes (history of diabetes/diabetes medication), current smoking and body mass index (BMI).

### 2.3. MRI acquisition

Patients underwent brain imaging on a 3.0 Tesla MR scanner (Achieva TX, Philips Healthcare, Best, the Netherlands) using a 32-element head coil suitable for parallel imaging. For anatomical segmentation a T1-weighted sequence (TR/TI/TE = 8.3/800/3.8 ms; FOV 256 × 256 × 160 $mm^3$; 1.0 $mm^3$ isotropic voxel) and a T2-weighted FLAIR sequence (TR/TI/TE = 4800/1650/299 ms; FOV 256 × 256 × 180 $mm^3$; 1.0 mm isotropic voxel) were performed respectively.

IVIM imaging was conducted as described before (van Bussel et al., 2015). In brief, a Stejskal-Tanner diffusion weighted (DW) spin echo single shot echo planar imaging pulse sequence (TR/TE = 6800/84 ms; FOV 221 × 269 × 139 $mm^3$; 2.4 mm isotropic voxel; acquisition time 5:13 min) was used. To minimize the signal contamination of CSF, an inversion recovery pulse (TI = 2230 ms) was given prior to the DW sequence (Hales & Clark, 2012). Fifteen DW images were acquired in the anterior-posterior direction using multiple diffusion sensitive *b*-values (0, 5, 7, 10, 15, 20, 30, 40, 50, 60, 100, 200, 400, 700, and 1000 s/$mm^2$). To increase the signal-to-noise ratio (SNR) (Appendix 1.2) at high *b*-values the number of signal averages for the highest two *b*-values were two and three, instead of one, respectively.

### 2.4. Image analysis

#### 2.4.1. Brain segmentation

The regions of interest (ROIs) were: the normal appearing white matter (NAWM), WMHs, deep grey matter (DGM) and the cortex. All ROIs were automatically segmented on T1-weighted images (Freesurfer software (Fischl et al., 2002) and FSL (v5.0) (Jenkinson et al., 2002)). The WMHs were automatically segmented (de Boer et al., 2009) on FLAIR images and visually checked under supervision of vascular neurologists, who also identified and excluded infarcts and scored PVS (Appendix 1.3). The WMH load was calculated by normalizing the WMH volume to the intracranial volume.

#### 2.4.2. IVIM analysis

Preprocessing of the IVIM images has been described previously (van Bussel et al., 2015) and consisted of distortion corrections (EPI and eddy current distortions) and head displacements (ExploreDTI v.4.8.3) (Leemans et al., 2009). Hereafter, the images were registered to the corresponding T1-weighted image and spatially smoothed with a 3 mm full-width-at-half-maximum Gaussian kernel. The SNR at $b$ = 1000 s/$mm^2$ was 45 (Association NEM, 2008) (Appendix 1.2), which is larger than the minimum value (i.e. 30) recommended for accurate IVIM estimation (Wu et al., 2015).

The diffusion-attenuation curve is approximated with a two-compartment diffusion model (Le Bihan et al., 1988):

$$\frac{S(b)}{S_0} = (1-f)e^{-bD} + fe^{-b(D^*+D)} \quad (1)$$

where $S_0$ is the signal intensity $S$ at *b*-value 0 s/$mm^2$, $S(b)$ the signal intensity at *b*-value $b$, $f$ the perfusion volume fraction, $D$ the parenchymal diffusivity and $D^*$ the pseudodiffusion coefficient. The IVIM model considers the presence of a vascular and non-vascular compartment. The vascular part embodies the fast water motion in blood flowing into a network of small vessels, which has an architecture with many microvessel orientations. This gives rise to the pseudodiffusion coefficient, hereafter called intravascular diffusivity $D^*$, and the perfusion volume fraction $f$. The perfusion related measure $f{\cdot}D^*$ was obtained by taking the product $f{\cdot}D^*$. The non-vascular compartment is described by the water diffusion in the parenchymal microstructure represented by the slower parenchymal diffusivity $D$. To account for the CSF suppression and differences in relaxation time of blood and tissue, a modified IVIM model (Hales & Clark, 2012) was employed (Appendix 1.4).

Model fitting was performed on a voxel-by-voxel basis using a two-step method (Federau et al., 2014) (Appendix 1.5). This yields the IVIM measures ($f$, $D^*$, $f{\cdot}D^*$ and $D$), which were averaged over each ROI. The analysis accounted for the goodness of fit of the model (Appendix 1.5).

### 2.5. Statistical analysis

To examine differences between cSVD patients and controls, independent Student's *t*-test and $\chi^2$ test were used where appropriate. The differences in IVIM measures between cSVD patients and controls

were analysed with an independent Student's *t*-test and multivariable linear regression analysis corrected for age, sex and cardiovascular factors. In addition, differences were tested between patients with lacunar stroke and mVCI. To account for multiple comparisons a false discovery rate of 10% was applied (Benjamini & Hochberg, 1995).

To investigate the relation between IVIM measures and disease severity on MRI, the WMH load was used as the dependent variable in linear regression. Both univariable and multivariable analyses with age, sex and cardiovascular factors were performed. This was conducted in patients, only for the IVIM measures that differed between patients and controls. Significance was inferred for $p < 0.05$. All statistical analyses were performed using SPSS (version 22, IBM Corp., USA).

## 3. Results

For this study 73 patients with cSVD (40 patients with lacunar stroke and 33 patients with mVCI), and 39 controls were suitable for analysis. Participants showing image artifacts and image processing complications (n = 11) were excluded (Appendix 1.6). Table 1 lists the characteristics of the participants. Patients and controls were well matched on age and sex. Patients were more often smokers, suffered more from hypercholesterolemia and had a lower BMI than controls. They also had a higher WMH load and more enlarged PVS in the basal ganglia. In Appendix Table 1 characteristics of patients with lacunar stroke and mVCI are shown. Patients with mVCI were older, suffered more from hypercholesterolemia and had a higher WMH load than those with lacunar stroke.

IVIM maps of a patient with cSVD and a control can be appreciated in Fig. 1. Table 2 shows the results of the perfusion volume fraction *f* and parenchymal diffusivity *D* in various ROIs. Patients have significantly higher perfusion volume fraction *f* than controls in all ROIs except in the WMHs. This difference remained significant after adjusting for age, sex and cardiovascular factors in the NAWM and DGM. Results of additional correction for medication and the extent of PVS can be found in Appendixes 1.3 and 1.7, respectively.

Higher parenchymal diffusivity *D* was found in all ROIs for patients compared with controls. Parenchymal diffusivity *D* remained higher for patients after adjusting for age, sex and cardiovascular factors.

The results for the intravascular diffusivity $D^*$ and perfusion-related measure $f{\cdot}D^*$ are provided in Appendix Table 2. No significant differences between the two groups were found for the intravascular diffusivity $D^*$ or the perfusion-related measure $f{\cdot}D^*$.

**Table 1**
Baseline characteristics of patients with cSVD and controls.

| | cSVD (n = 73) | Controls (n = 39) | *p*-Value[c] |
|---|---|---|---|
| Age, y, mean(SD) | 70(11) | 69(12) | 0.49 |
| Male, n(%) | 43(59) | 23(59) | 0.99 |
| Hypertension, n(%) | 46(42) | 18(46) | 0.09 |
| Hypercholesterolemia, n(%) | 47(64) | 13(33) | <**0.01** |
| Diabetes Mellitus, n(%) | 12(16) | 4(10) | 0.57 |
| Smoking, n(%) | 18(25) | 3(7.7) | **0.04** |
| Body mass index, mean(SD) | 25(3.9) | 27(3.5) | **0.04** |
| Education[a] | | | 0.26 |
| High, n(%) | 13(18) | 6(15) | |
| Moderate, n(%) | 26(36) | 20(51) | |
| Low, n(%) | 34(47) | 13(33) | |
| Calcium antagonists intake (n%) | 14(19) | 4(10) | 0.29 |
| WMH load, mean (SD) $\times 10^{-3}$ | 14(15) | 5.0(9.8) | <**0.001** |
| Presence of severe PVS[b] | | | |
| Centrum semiovale n(%) | 30(48) | 13(37) | 0.32 |
| Basal ganglia n(%) | 17(27) | 2(5.1) | **0.02** |

Abbreviations: WMH = white matter hyperintensity; PVS = perivascular spaces.
Bold values indicate significance at p <0.05.
[a] Education level: low: finished high school or lower; moderate: finished intermediate vocational education; high: finished university degree (Verhage, 1964).
[b] These values represent participants with >25 PVS (Appendix 1.3).
[c] *t*-Test or chi-square.

Comparison between patients with lacunar stroke and mVCI are shown in Appendix Tables 3 and 4. Patient with mVCI had higher perfusion volume fraction *f* ($p = 0.01$), intravascular diffusivity $D^*$ ($p = 0.02$) and perfusion-related measure $f{\cdot}D^*$ ($p \leq 0.01$) than patients with lacunar stroke in the DGM using univariable linear regression. Furthermore, higher parenchymal diffusivity *D* was observed in the NAWM for patients with mVCI than with lacunar stroke. However, when adjusting for cardiovascular risk factors and multiple comparisons, none of these differences remained significant.

Table 3 and Fig. 2 show the relation of the perfusion volume fraction *f* and the parenchymal diffusivity *D* with the WMH load in patients. Higher *D* in all ROIs was significantly associated with higher WMH load. Accounting for confounding effects of age, sex, and cardiovascular factors, the association weakened but remained significant. For the perfusion volume fraction *f*, a positive association with the WMH load was also present in all ROIs except in the WMHs. Moreover, this association remained significant (though slightly weaker) after adjusting for age, sex and cardiovascular factors.

## 4. Discussion

In this study, IVIM imaging was applied in cSVD for the first time. We showed that patients with cSVD exhibit a larger perfusion volume fraction *f* and a higher parenchymal diffusivity *D* in the normal appearing brain tissue (i.e. NAWM, DGM and cortex) than controls. These IVIM measures were also associated with the severity of WMH on MRI.

A higher parenchymal diffusivity for patients is in good accordance with previous studies (Chabriat et al., 1999; O'Sullivan et al., 2001; Molko et al., 2001). This measure is comparable with the better-known mean diffusivity, though without contaminating effects of the microvasculature. Higher mean diffusivity was proposed to indicate microstructural changes in tissue involving the loss of structural barriers and the increase of extracellular space (Jones et al., 1999; Chabriat et al., 1999). In our study, higher parenchymal diffusivity, and its association with the disease severity, suggest that changes in the parenchymal microstructure, which are not yet visible on conventional T2-weighted images (Fig. 1), are present in areas that may be vulnerable for potential future damage. Previously, a correlation between increased mean diffusivity and clinical disease severity was found in patients with cerebral autosomal-dominant arteriopathy with subcortical infarcts and leukoencephalopathy (CADASIL) (Chabriat et al., 1999) using DTI.

On the contrary, our observations in the microvasculature differ with results of previous studies using other MR techniques. Reduced perfusion has been reported for patients with cSVD (Chabriat et al., 1999; O'Sullivan et al., 2001), while we found a larger perfusion volume fraction *f*. The interpretation of the perfusion volume fraction *f* is not trivial. However, the vascular nature of *f* has been demonstrated previously. Several studies have shown a good correlation between the perfusion volume fraction *f* and the cerebral blood volume using the more standard dynamic susceptibility contrast imaging (Wu et al., 2015; Federau et al., 2014; Wirestam et al., 2001). In addition, a phantom study reported that *f* correlated well with flow (Lee et al., 2016).

By definition, the perfusion volume fraction *f* is proportional to the ratio between the signal contribution from the slow diffusing water in the parenchyma and the fast diffusion arising from flowing water in the microvasculature mimicking a random walk. Several factors that might contribute to the fast diffusing component, which can lead to an increased perfusion volume fraction *f*, are discussed.

Firstly, the seemingly most straightforward explanation is that more water molecules flow through the microvascular network that contributes to the fast component. This can be interpreted as a network with more dilated vessels. Vasodilation might be present for patients either as a physical compensatory mechanism or as an action of antihypertensive calcium antagonists, the latter are known to act on the vascular smooth muscle cells causing vasodilation (Russell, 1988). A trend of larger perfusion volume fraction *f* was indeed observed for those using

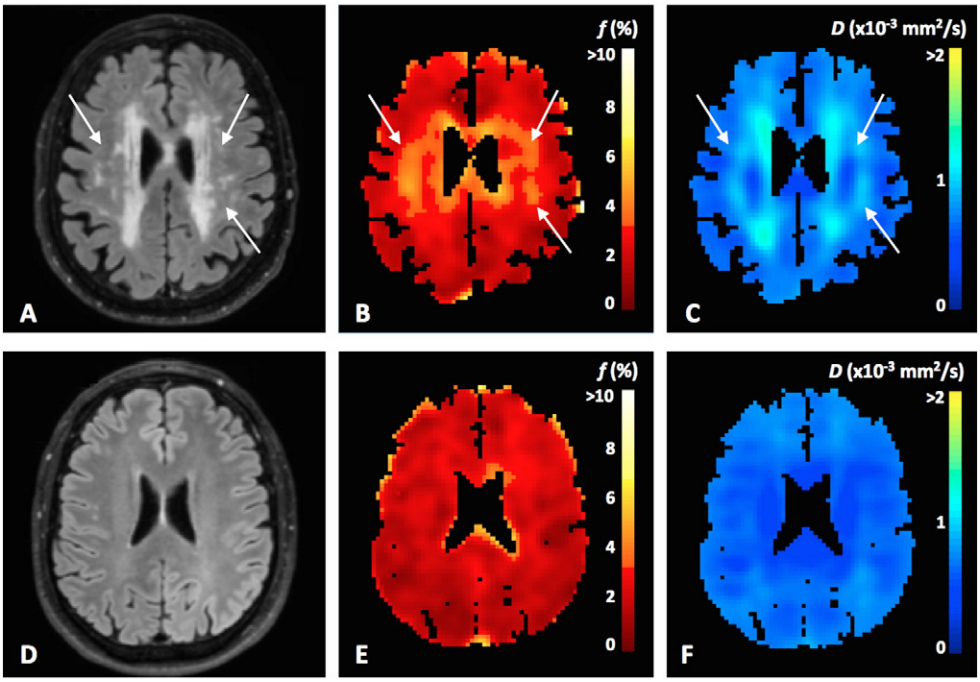


**Fig. 1.** Example of a FLAIR image (A,D) and IVIM maps of the perfusion volume fraction *f* (B, E) and parenchymal diffusivity *D* (C,F) for a patient with cSVD (A, B C) and a control (D, E, F), respectively. The arrows in the images in the upper row indicate tissue with high values of perfusion volume fraction *f* and parenchymal diffusivity *D*, which appears normal on the FLAIR image (A). Note that the FLAIR images have a higher resolution (1 $mm^3$ isotropic) than the IVIM maps (2.4 $mm^3$ isotropic).

calcium antagonists (Appendix 1.7). After adjusting for these drugs, patients with cSVD still had a larger perfusion volume fraction *f* than controls, which indicates that vasodilation due to medication might only explain the larger *f* in some degree.

Secondly, water flowing in another compartment, parallel to the microvasculature that follows the blood flow in the random network can also contribute to the fast diffusing component. Enlarged PVS corresponds with this thought, which in cSVD is caused by leakage of plasma into the perivascular space through an impaired blood brain barrier (Wardlaw et al., 2013b; Potter et al., 2013). Indeed, a larger perfusion volume fraction *f* is associated with higher PVS score (Appendix 1.3). To further investigate its contribution, linear regression was adjusted for enlarged PVS. Patients still had a larger perfusion volume fraction *f*, but enlarged PVS remained a significant confounder indicating that it partly explains the larger *f*.

Thirdly, water molecules that change more directions can increase the signal attenuation that contributes to the fast component. This can be depicted as increased vessel tortuosity. Previously, increased tortuosity has been shown in cSVD using histology (e.g. the retina and cerebral arteries) (Wardlaw & Pantoni, 2014; Brown & Thore, 2011; Hilal et al., 2014; Ong et al., 2013).

Briefly, previous studies have demonstrated the microvascular nature of the perfusion volume fraction *f*. Although the interpretation of the perfusion volume fraction *f* is complex, we have proposed three possible factors for an increased *f*. Future studies are needed to investigate this in more details. Furthermore, based on the observed correlation of a larger *f* with the severity of WMH in our study, it can be hypothesized that regions with a larger *f* might be indicative of areas at risk for (later) damage, which are not yet visible on conventional T2-weighted images (Fig. 1).

**Table 2**
Perfusion volume fraction *f* and parenchymal diffusivity *D* of patients and controls.

| | cSVD (n = 73) | Controls (n = 39) | Model 1[a] ΔMean(95% CI)[d] | *p*-Value | Model 2[b] *β*(95% CI)[e] | *p*-Value | $R^2$ |
|---|---|---|---|---|---|---|---|
| Perfusion volume fraction $f \times 10^{-2}$ (SE) | | | | | | | |
| NAWM | 2.31(0.03) | 2.21(0.03) | 0.11(0.03, 0.20) | **0.011**[c] | 0.48(0.08, 0.88) | **0.020**[c] | 0.197 |
| DGM | 2.95(0.04) | 2.69(0.05) | 0.26(0.12, 0.39) | <**0.001**[c] | 0.68(0.29, 1.07) | **0.001**[c] | 0.247 |
| Cortex | 2.53(0.04) | 2.40(0.04) | 0.14(0.02, 0.26) | **0.024**[c] | 0.39(−0.02, 0.79) | 0.060 | 0.184 |
| WMHs | 3.21(0.04) | 3.03(0.09) | 0.19(0.02, 0.39) | 0.076 | 0.38(−0.03, 0.78) | 0.068 | 0.158 |
| Parenchymal diffusivity $D \times 10^{-4}$ (SE) $mm^2/s$ | | | | | | | |
| NAWM | 7.35(0.04) | 7.15(0.05) | 0.20(0.08, 0.32) | **0.002**[c] | 0.56(0.18, 0.93) | **0.004**[c] | 0.325 |
| DGM | 7.77(0.05) | 7.54(0.05) | 0.24(0.08, 0.39) | **0.003**[c] | 0.44(0.07, 0.82) | **0.020**[c] | 0.329 |
| Cortex | 7.40(0.02) | 7.30(0.03) | 0.10(0.02, 0.18) | **0.012**[c] | 0.45(0.04, 0.86) | **0.030**[c] | 0.191 |
| WMHs | 9.38(0.11) | 8.93(0.19) | 0.45(0.04, 0.86) | **0.031**[c] | 0.50(0.11, 0.88) | **0.012**[c] | 0.264 |

NAWM = normal appearing white matter; DGM = deep grey matter; WMHs = white matter hyperintensities; SE = standard error; CI = confidence interval; $R^2$ = R-squared of the linear regression model.

[a] Unadjusted Student's *t*-test.

[b] Linear regression adjusted for age, sex, and cardiovascular factors.

[c] Remained significant after testing for multiple comparisons.

[d] ΔMean refers to the differences in mean of the IVIM parameter between the cSVD and control group.

[e] *β* is the regression coefficient of the independent variable group (0 = control; 1 = cSVD) in the multivariable regression model.

**Table 3**
Association of perfusion volume fraction *f* and parenchymal diffusivity *D* with the WMH load in patients with cSVD.

| | Model 1[a] $\beta$(95% CI)[c] | *p*-Value | $R^2$ | Model 2[b] $\beta$(95% CI)[c] | *p*-Value | $R^2$ |
|---|---|---|---|---|---|---|
| Perfusion volume fraction *f* | | | | | | |
| NAWM | 1.89(0.51, 3.27) | <**0.01** | 0.095 | 1.49(0.21, 2.78) | **0.024** | 0.389 |
| DGM | 1.86(1.00, 2.72) | <**0.001** | 0.207 | 1.14(0.23, 2.05) | **0.015** | 0.397 |
| Cortex | 1.58(0.57, 2.59) | <**0.01** | 0.121 | 1.19(0.25, 2.13) | **0.014** | 0.398 |
| WMHs | 0.13(−0.87, 1.13) | 0.794 | 0.132 | −0.02(−0.94, 0.91) | 0.972 | 0.328 |
| Parenchymal diffusivity *D* | | | | | | |
| NAWM | 311(227, 395) | <**0.001** | 0.436 | 253 (153, 353) | <**0.001** | 0.529 |
| DGM | 221(155, 287) | <**0.001** | 0.384 | 178 (103,252) | <**0.001** | 0.513 |
| Cortex | 406 (273, 539) | <**0.001** | 0.342 | 302(162, 443) | <**0.001** | 0.488 |
| WMHs | 105 (78,132) | <**0.001** | 0.455 | 97 (66, 128) | <**0.001** | 0.588 |

NAWM = normal appearing white matter; DGM = deep grey matter; WMHs = white matter hyperintensities; CI = confidence interval; $R^2$ = R-squared of the linear regression model.
Bold values indicate significance at $p < 0.05$.
[a] Unadjusted Student's *t*-test.
[b] Linear regression adjusted for age, sex, and cardiovascular factors.
[c] $\beta$ is the regression coefficient of the IVIM parameter (*f* or *D*) in the multivariable regression model where WMH load is the dependent variable.

The strength of the current study is that it was performed in a well-defined cSVD group, which indicates that findings can be clearly related to cSVD, and effects of confounders have been controlled for. Moreover, in contrast with mean diffusivity, the IVIM-derived parenchymal diffusivity *D* is without contaminating effects of the microvasculature and therefore provides a more accurate measure for the parenchymal integrity. Furthermore, IVIM provides the opportunity to assess the perfusion and diffusion without the use of a contrast agent, which is relevant for patients with impaired kidney function (Makin et al., 2015; Ikram et al., 2008). In addition, an inversion recovery pre-pulse was applied to minimize contamination from CSF to ensure accurate calculation of the IVIM measures.

However, this study also has a few limitations. Firstly, the IVIM technique assumes a two-compartment model, which might be an oversimplification of the actual underlying structure and also for pathological regions (i.e. WMHs) (Appendix 1.5). Secondly, we performed IVIM imaging in one direction. Imaging in more directions can provide more information on the directionality of the white matter. However, the longer scan times needed for more directions also substantially decrease patient comfort and may cause more motion artifacts. Thirdly, carotid imaging was performed to ensure changes in the small vessels were not due to large vessel pathology. We cannot fully exclude that patients with mVCI and controls had no carotid stenosis, since no carotid imaging was performed for these participants. In addition, we do not know the precise effect of carotid stenosis on the IVIM parameters. Future studies are needed to examine their relation. Lastly, patients with mVCI may have coexisting pathologies in addition to cSVD, for example neurodegeneration (e.g. Alzheimer's disease). To prevent contamination as much as possible, we tried to select only the patients that were diagnosed with mVCI most probably due to cSVD. This diagnosis was given after extensive evaluation of patient history, physical examination, neuropsychological assessment and MRI scans. Furthermore, patients showing evident atrophy in the hippocampi on MR images, which are one of the hallmarks of Alzheimer's disease, were excluded.

To conclude, we demonstrated the first application of IVIM in cSVD. The increased parenchymal diffusivity *D* reflects the expected microstructural impairment in cSVD. However, the increased perfusion volume fraction *f* is not fully in agreement with the reported hypoperfusion in cSVD. Cautious interpretation of the perfusion volume fraction *f* in cSVD is needed, as *f* might not be purely blood flow-related. Future studies are needed to investigate this. Nevertheless, IVIM imaging showed abnormalities in both the parenchymal diffusivity *D* and perfusion volume fraction *f*, which increased with disease severity. This

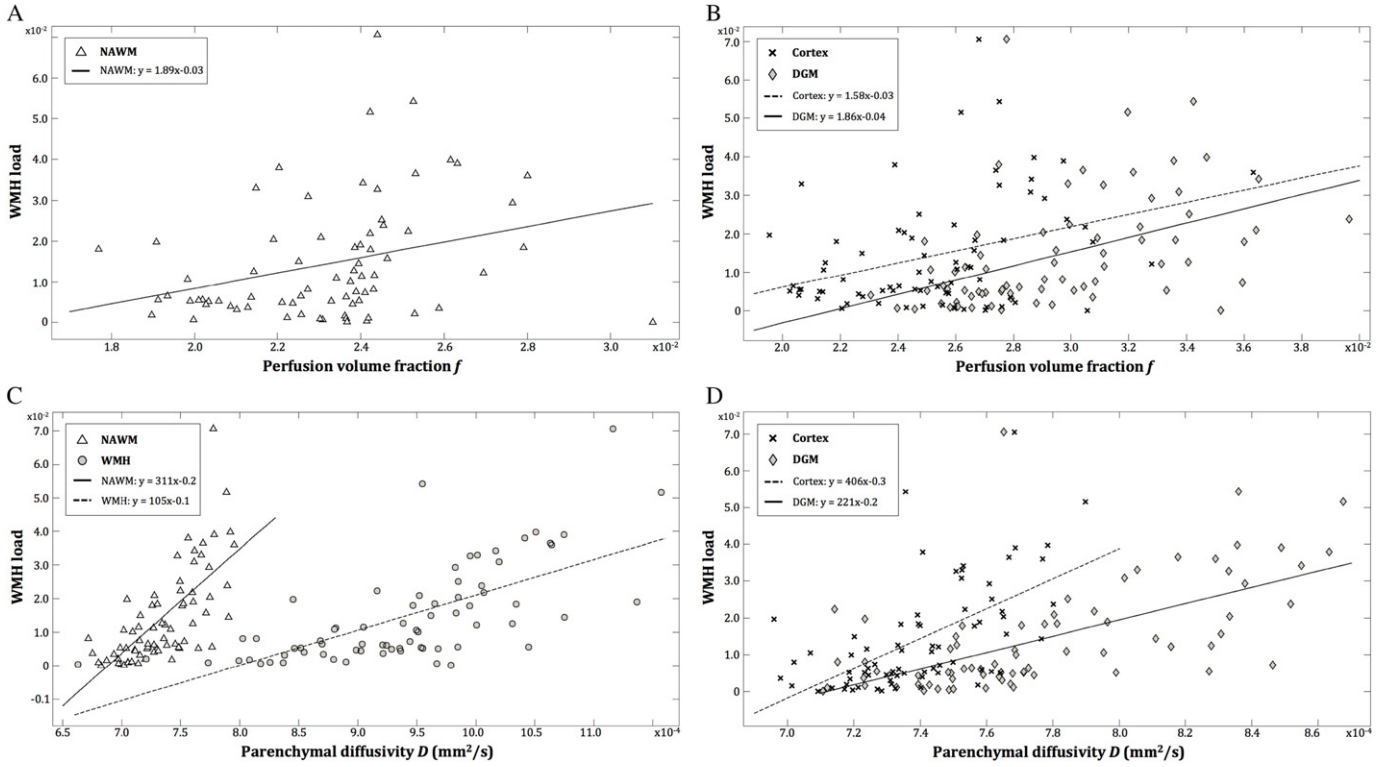


**Fig. 2.** Association between the WMH load and the IVIM parameters *f* and *D*. Scatterplots showing the unadjusted correlation between the WMH load and perfusion volume fraction *f* (A and B), and parenchymal diffusivity *D* (C and D) in the white matter (NAWM: white triangles; WMH: grey circles) and in the grey matter (B) (DGM: grey diamonds; cortex: black crosses). The WMH load increases significantly with higher perfusion volume fraction *f* in the NAWM (A), DGM and cortex (B). The same effect was observed for parenchymal diffusivity *D* in the NAWM and WMH (C), and DGM and cortex (D).

indicates the potential of IVIM imaging to provide a surrogate marker for the progression of cSVD.

## 5. Acknowledgement

Funding: SMW was funded by 'Academisch Fonds' of Maastricht University Medical Centre and by 'Stichting de Weijerhorst' Foundation. CEZ was funded by the Mosaic program of The Netherlands Organisation for Scientific Research (NWO) (Grant: 017.009.048) and 'de Hersenstichting' (Grant: 2013(1)-195).

## Appendix A. Supplementary data

Supplementary data to this article can be found online at http://dx.doi.org/10.1016/j.nicl.2017.01.017.

## References

Association NEM, 2008. Determination of Signal-to-Noise Ration (SNR) in Diagnostic Magnetic Resonance Imaging. NEMA Stand Publ MS1.
Bamford, J., Sandercock, P., Jones, L., Warlow, C., 1987. The natural history of lacunar infarction: the Oxfordshire Community Stroke Project. Stroke 18, 545–551.
Benjamini, Y., Hochberg, Y., 1995. Controlling the false discovery rate: a practical and powerful approach to multiple testing. J. R. Stat. Soc. 289–300.
Brown, W.R., Thore, C.R., 2011. Review: cerebral microvascular pathology in ageing and neurodegeneration. Neuropathol. Appl. Neurobiol. 37, 56–74.
Chabriat, H., Pappata, S., Poupon, C., et al., 1999. Clinical severity in CADASIL related to ultrastructural damage in white matter: in vivo study with diffusion tensor MRI. Stroke 30, 2637–2643.
de Boer, R., Vrooman, H., van der Lijn, F., et al., 2009. White matter lesion extension to automatic brain tissue segmentation on MRI. NeuroImage Elsevier Inc. 45, 1151–1161.
Federau, C., O'Brien, K., Meuli, R., Hagmann, P., Maeder, P., 2014. Measuring brain perfusion with intravoxel incoherent motion (IVIM): initial clinical experience. J. Magn. Reson. Imaging 39, 624–632.
Fischl, B., Salat, D.H., Busa, E., et al., 2002. Whole brain segmentation: automated labeling of neuroanatomical structures in the human brain. Neuron 33, 341–355.
Gorelick, P.B., Scuteri, A., Black, S.E., et al., 2011. Vascular contributions to cognitive impairment and dementia: a statement for healthcare professionals from the American Heart Association/American Stroke Association. Stroke 42, 2672–2713.
Hales, P.W., Clark, C., 2012. Combined arterial spin labeling and diffusion-weighted imaging for noninvasive estimation of capillary volume fraction and permeability-surface product in the human brain. J. Cereb. Blood Flow Metab. 67–75.
Hilal, S., Ong, Y.T., Cheung, C.Y., et al., 2014. Microvascular network alterations in retina of subjects with cerebral small vessel disease. Neurosci. Lett. Elsevier Ireland Ltd 577, 95–100.
Iima, M., Le Bihan, D, 2016. Clinical Intravoxel Incoherent Motion and Diffusion MR. 278.
Ikram, M.A., Vernooij, M.W., Hofman, A., Niessen, W.J., Van Der Lugt, A., Breteler, M.M.B., 2008. Kidney function is related to cerebral small vessel disease. Stroke 39, 55–61.
Jenkinson, M., Bannister, P., Brady, M., Smith, S., 2002. Improved optimization for the robust and accurate linear registration and motion correction of brain images. NeuroImage 17, 825–841.
Jones, D.K., Lythgoe, D., Horsfield, M., Simmons, A., Williams, S.C., Markus, H.S., 1999. Characterization of white matter damage in ischemic leukoaraiosis with diffusion tensor MRI. Stroke 30, 393–397.
Le Bihan, D., Breton, E., Lallemand, D., 1988. Separation of diffusion and perfusion in Intravoxel incoherent motion MR imaging. Radiology 497–505.
Lee, J.H., Cheong, H., Lee, S.S., et al., 2016. Perfusion assessment using intravoxel incoherent motion-based analysis of diffusion-weighted magnetic resonance imaging. Investig. Radiol. 51, 520–528.
Leemans, A., Jeurissen, B., Sijbers, J., Jones, D., 2009. ExploreDTI: a graphical toolbox for processing, analyzing, and visualizing diffusion MR data. Proc 17th Sci Meet Int Soc Magn Reson Med. 17, p. 3537.
Makin, S.D.J., Cook, F.A.B., Dennis, M.S., Wardlaw, J.M., Wardlaw, J.M., 2015. Cerebral small vessel disease and renal function: systematic review and meta-analysis. Cerebrovasc. Dis. 3939, 39–52.
Makin, S.D.J., Turpin, S., Dennis, M.S., Wardlaw, J.M., 2013. Cognitive impairment after lacunar stroke: systematic review and meta-analysis of incidence, prevalence and comparison with other stroke subtypes. J. Neurol. Neurosurg. Psychiatry 84, 893–900.
Markus, H.S., Lythgoe, D.J., Ostegaard, L., O'Sullivan, M., Williams, S.C., 2000. Reduced cerebral blood flow in white matter in ischaemic leukoaraiosis demonstrated using quantitative exogenous contrast based perfusion MRI. J. Neurol. Neurosurg. Psychiatry 69, 48–53.
Molko, N., Pappata, S., Mangin, J.F., et al., 2001. Diffusion tensor imaging study of subcortical gray matter in cadasil. Stroke 32, 2049–2054.
Ong, Y.T., De Silva, D.A., Cheung, C.Y., et al., 2013. Microvascular structure and network in the retina of patients with ischemic stroke. Stroke 44, 2121–2127.
O'Sullivan, M., Lythgoe, D.J., Pereira, C., et al., 2002. Patterns of cerebral blood flow reduction in patients with ischemic leukoaraiosis. Neurology 59, 321–326.
O'Sullivan, M., Summers, P.E., Jones, D.K., Jarosz, J.M., Williams, S.C., Markus, H.S., 2001. Normal-appearing white matter in ischemic leukoaraiosis: a diffusion tensor MRI study. Neurology 57, 2307–2310.
Pantoni, L., 2010. Cerebral small vessel disease: from pathogenesis and clinical characteristics to therapeutic challenges. Lancet Neurol. 9, 689–701.
Pantoni, L., Gorelick, P., 2011. Advances in vascular cognitive impairment 2010. Stroke 42, 291–293.
Potter, G.M., Doubal, F.N., Jackson, C.A., et al., 2013. Enlarged perivascular spaces and cerebral small vessel disease. Int. J. Stroke 1–6.
Russell, R.P., 1988. Side effects of calcium channel blockers. Hypertension 11, 42–44.
van Bussel, F.C., Backes, W.H., Hofman, P.A., et al., 2015. On the interplay of microvasculature, parenchyma, and memory in type 2 diabetes. Diabetes Care 38, 876–882.
Verhage, F., 1964. Intelligentie en leeftijd bij volwassenen en bejaarden. Koninklijke Van Gorcum.
Wardlaw, J.M., Pantoni, L., 2014. Sporadic small vessel disease: pathogenic aspects. In: Pantoni, L., Gorelick, P. (Eds.), Cereb Small Vessel Dis, first ed. Cambridge University Press, Cambridge, pp. 52–63.
Wardlaw, J.M., Smith, C., 2013. Mechanisms underlying sporadic cerebral small vessel disease: insights from neuroimaging. Lancet Neurol. 12, 483–497.
Wardlaw, J.M., Doubal, F.N., Valdes-Hernandez, M., et al., 2013a. Blood-brain barrier permeability and long-term clinical and imaging outcomes in cerebral small vessel disease. Stroke 44, 525–527.
Wardlaw, J.M., Smith, E.E., Biessels, G.J., et al., 2013b. Neuroimaging standards for research into small vessel disease and its contribution to ageing and neurodegeneration. Lancet Neurol. 12, 822–838.
Wirestam, R., Borg, M., Brockstedt, S., Lindgren, A., Holtås, S., Ståhlberg, F., 2001. Perfusion-related parameters in intravoxel incoherent motion Mr imaging compared with Cbv and Cbf measured by dynamic susceptibility-contrast Mr technique. Acta Radiol. 42, 123–128.
Wu, W.C., Chen, Y.F., Tseng, H.M., Yang, S.C., My, P.C., 2015. Caveat of measuring perfusion indexes using intravoxel incoherent motion magnetic resonance imaging in the human brain. Eur. Radiol. 2485–2492.